PROCEEDINGS OF THE ROYAL SOCIETY A

rspa.royalsocietypublishing.org

The available power from tidal stream turbines in the Pentland Firth

Thomas A. A. Adcock[1], Scott Draper[2], Guy T. Houlsby[1], Alistair G. L. Borthwick[3] and Sena Serhadlıoğlu[1]

[1]Department of Engineering Science, University of Oxford, Oxford OX1 3PJ, UK

[2]Centre for Offshore Foundation Systems, University of Western Australia, Crawley, Western Australia 6009, Australia

[3]Department of Civil and Environmental Engineering, University College Cork, Cork, Republic of Ireland

Research

Cite this article: Adcock TAA, Draper S, Houlsby GT, Borthwick AGL, Serhadlıoğlu S. 2013 The available power from tidal stream turbines in the Pentland Firth. Proc R Soc A 469: 20130072.
http://dx.doi.org/10.1098/rspa.2013.0072

Received: 3 February 2013
Accepted: 13 June 2013

Subject Areas:
energy, ocean engineering

Keywords:
tidal stream energy, resource assessment, Pentland Firth, available power

Author for correspondence:
Thomas A. A. Adcock
e-mail: thomas.adcock@st-peters.oxon.org

This paper assesses an upper bound for the tidal stream power resource of the Pentland Firth. A depth-averaged numerical model of the tidal dynamics in the region is set-up and validated against field measurements. Actuator disc theory is used to model the effect of turbines on the flow, and to estimate the power available for generation after accounting for losses owing to mixing downstream of the turbines. It is found that three rows of turbines extending across the entire width of the Pentland Firth and blocking a large fraction of the channel can theoretically generate 1.9 GW, averaged over the spring–neap cycle. However, generation of significantly more power than this is unlikely to be feasible as the available power per additional swept area of turbine is too small to be viable. Our results differ from those obtained using simplified tidal channel models of the type used commonly in the literature. We also use our numerical model to investigate the available power from rows of turbines placed across various subchannels within the Pentland Firth, together with practical considerations such as the variation in power over the spring–neap tidal cycle and the changes to natural tidal flows which result from power extraction.

Royal Society Publishing
Informing the science of the future

1. Introduction

The Pentland Firth is the strait connecting the Atlantic Ocean to the North Sea between mainland Scotland and the Orkney Isles. The strait is well known to have exceptionally fast tidal currents, and has become a focal point for tidal stream power device developers. The tidal currents, which can exceed $5\,\mathrm{m\,s^{-1}}$, are principally due to the phase difference in water level across the Pentland Firth, established as the tide propagates from the Atlantic Ocean and around the Orkney Isles into the North Sea. However, despite the potential importance of the site to tidal stream power generation, no robust calculation has been made of the power which could be generated from the Pentland Firth. Estimates of how much power might be generated vary considerably from 1 GW averaged over the tidal cycle [1] to approximately 18 GW at peak flow [2]. However, the methodology underpinning these estimates has been shown to be flawed [3]. More recently, Vennell [4] used a simple tidal channel model (solely accounting for M_2 tides) to analyse various configurations of turbines in a channel loosely based on the Pentland Firth and suggested that a feasible development might have a peak available power of 1.8 GW.

The main purpose of this paper is to calculate an upper bound on the power which may be generated from the Pentland Firth using tidal stream turbines in order to assess the magnitude of the resource. Our aim is to refine the traditional upper bound estimate to power generation from a tidal channel, known as the power potential or maximum time-averaged power that can be extracted from the channel (as defined by [3]). To do this, we consider the time-averaged available power which can be removed or generated by discrete rows of turbines deployed across the Pentland Firth, in which the available power is defined as the fraction of extracted power that can be removed by tidal turbines. We choose to estimate this available power using a quasi-inviscid actuator disc model of an ideal tidal turbine, which accounts for the energy loss owing to mixing in the wake of the turbine [5,6], but not other mechanical and electrical losses, or the drag owing to the support structure of the turbine. In adopting this approach, we assume that the actuator disc model overestimates the available power that an actual turbine may generate for an equivalent drag or retarding force on the flow.

To calculate both the extractable and available power from the Pentland Firth, we use a depth-averaged numerical model to simulate the tidal hydrodynamics around the north of Scotland. Rows of tidal turbines in the Pentland Firth are introduced numerically, and we adjust the turbine properties within each row to maximize the power available for generation (following the approach of Vennell [7–10]). Different numbers of rows with different blockage ratios are considered, including rows of turbines across some of the subchannels formed by the islands of Swona and Stroma within the Pentland Firth.

Through explicitly modelling available power in this way, it is possible to calculate the extra power that is removed by each additional row of turbines placed in the Pentland Firth. Given that the additional power increment typically tails off as further rows of turbines are added [7], a law of diminishing returns applies limiting the number of additional rows of turbines that is likely to be feasible in the Pentland Firth. The cumulative generation from the rows up to this limit is therefore a more useful upper bound estimate of the power potential of a tidal channel, and will be necessarily lower than the traditional estimate of power potential based only on extracted power. Estimation of the revised upper bound is the main focus of this paper.

To determine whether or not an additional row of turbines is feasible in practice, it is necessary to carry out a full economic analysis that includes the capital and recurrent costs of the tidal turbines. However, because a full economic analysis is likely to be subjective and is well beyond the scope of this paper, we use an alternative (and arguably a more general) approach for assessing the limiting number of turbine rows based on the metric of time-averaged power per swept area of turbine. Our reasoning is that for deployment of a tidal turbine to be feasible it must, at least, generate a quantity of power per swept area that is larger than that of a typical offshore wind turbine, because the latter will be significantly cheaper owing to lower loading and easier maintenance.

2. Numerical model

(a) Numerical scheme

To simulate tidal flows in the Pentland Firth, we solve the shallow water equations using the discontinuous Galerkin (DG) version of ADCIRC [11,12]. This numerical scheme has been previously verified and validated for various applications such as modelling tidal flows and storm surges [13]. Our choice of numerical model is built on the fact that depth-averaged models have been shown by many authors to provide a reasonable representation of tidal dynamics on the continental shelf [14]. However, we also note that there are certain physical phenomena which the shallow water equations model poorly. An examination of some of the resulting limitations is given by Stansby [15]. In particular, depth-integrated schemes do not correctly capture the dynamics of turbulent mixing in the wakes of headlands or islands where the flow is sheared significantly in the horizontal plane. Depth-integrated schemes are also unable to capture velocity variations in the vertical direction owing to secondary flows which may form around the same coastal features, or from separation in the vertical plane near to abrupt bathymetric features. These flow features can, of course, affect larger-scale mixing and will lead to deviations between actual depth-averaged velocities and those predicted by a depth-averaged model. Because of these limitations, particular care must be taken when interpreting the results from depth-averaged models. In the present analysis, it is very likely that the physics may not be modelled correctly at all locations within the Pentland Firth. Nevertheless, the present model does show reasonable agreement with field data at various locations within the Firth (described in §3).

(b) Details of numerical model

Figure 1 shows the overall computational mesh used to model the Pentland Firth. Figure 2 presents detail of the mesh in the vicinity of the Firth itself. To simplify the meshing and to allow for efficient computation, the coastline was straightened in places, and small connecting channels removed where the cross-sectional area was less than 1% that of the main strait. The grid resolution varied from 150 m in the Pentland Firth to 20 km beyond the continental shelf. No wetting and drying was implemented, and so minor modifications to the shoreline were made to ensure elements did not become dry—the model was found to be insensitive to these modifications. The bathymetry data were purchased from Seazone. For the Pentland Firth and Orkney Islands, 'survey' data were provided at a spatial resolution of 2.78×10^{-4} degrees (approx. 30 m). Elsewhere in the domain, data interpolated from charts were supplied at a resolution of 1.7×10^{-3} degrees (approx. 180 m). At all locations, the bathymetry is much more finely resolved than the mesh.

The location of the open boundary is based on the analysis by Adcock *et al.* [16]. The offshore boundary is forced (i.e. prescribed) using elevation components taken from the model of le Provost *et al.* [17]. As pointed out by Garrett & Greenberg [18], prescription of the elevation at the boundary is wrong, in principle, as any changes to the tidal dynamics within the model should be allowed to cause a change at the free surface at the boundary. However, if the disturbance to the natural tidal dynamics at the boundary is small (and the boundary does not excite resonance in any of the principal tidal constituents or their harmonics; see [19]), then the error will be negligible. This was found to be the case here—even when the flow rate through the Pentland Firth was reduced to 25% of the natural value (as would occur in an unrealistically large deployment of tidal devices), the change in current at the boundary was less than 3% at any location (and at 90% of the boundary nodes the change was less than 0.5%). Moreover, the model has also been run with boundaries extending roughly half the distance from the Pentland Firth compared with those shown in figure 1. The power estimates predicted by the smaller domain model were very close to those obtained using the larger domain model. Thus, we are confident that no significant error has been introduced by our choice of location and treatment of the ocean boundary.

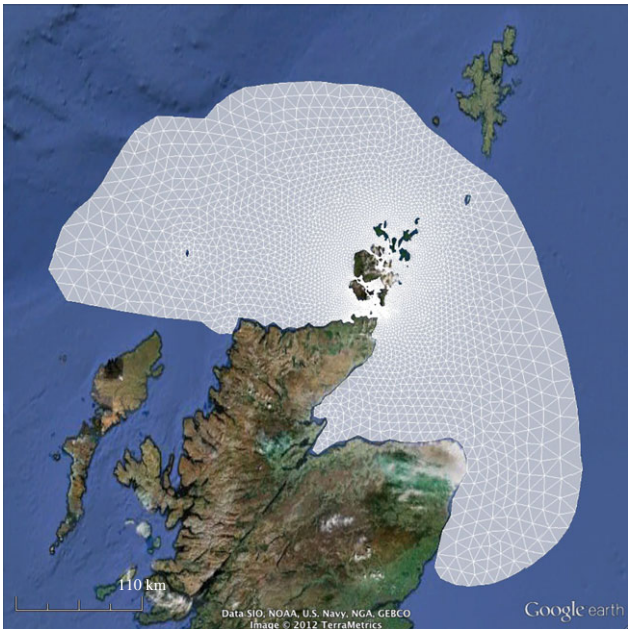

Figure 1. Mesh used for numerical simulation superimposed on image from Google Earth. (Online version in colour.)

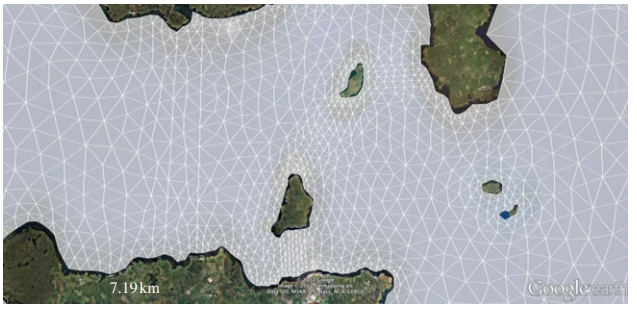

Figure 2. Detail of mesh used for numerical simulation superimposed on image from Google Earth. (Online version in colour.)

The drag resistance on the flow owing to bed friction is given by $\mathbf{F} = \frac{1}{2} C_d \rho A_b \mathbf{u}|\mathbf{u}|$, where A_b is the horizontal area of the seabed, ρ is density and $\mathbf{u}$ the depth-averaged velocity vector. Here, a constant value of bed friction coefficient was prescribed such that $C_d = 0.005$. Section 3*b* describes the rationale behind this choice. The value is similar to that used by Baston & Harris [20] but smaller than that used by Easton *et al.* [21], who used a different convention for the drag coefficient. It should be stressed that the bed friction value is very much model-dependent, and is a function of various numerical parameters such as grid size. Section 8*a* examines the sensitivity of the resource assessment to the bed friction parameter.

(c) Inclusion of tidal turbines

Tidal turbines are represented in the model as a line discontinuity in elevation following the method of Draper *et al.* [6] (see also figure 3). This method relates the water level downstream of a homogeneous row of turbines (once local mixing in the wake of a turbine has taken place) to the water level upstream, and describes a momentum 'sink' representative of the force (equal and opposite) applied by the turbine to the flow. If this force per unit length along the fence is defined

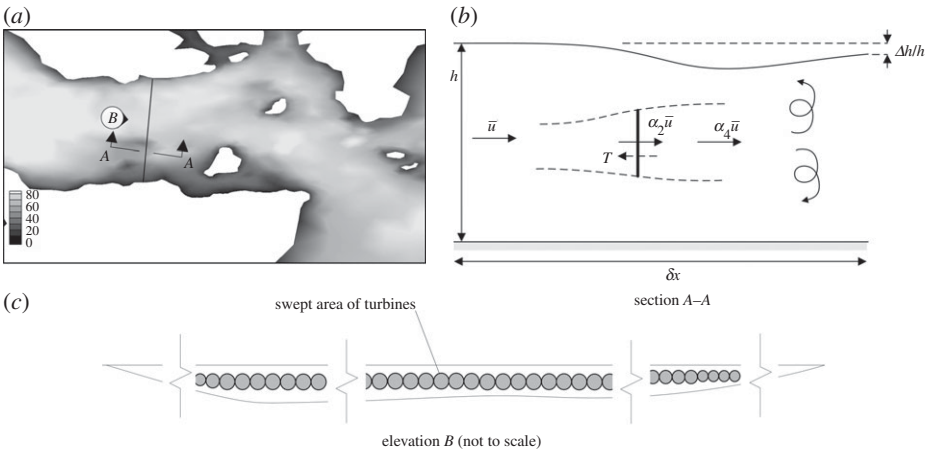

Figure 3. Schematic of the methodology used to include tidal turbines in the depth-averaged model. Solid line in (*a*) represents a row of tidal turbines. (*b*) Illustrates that a depth change $\Delta h/h$ occurs across the row following mixing in the wake of the devices. This mixing is assumed to occur over a distance δx sufficiently small that the change in depth occurs as a discontinuity across the line representing the row in the model.

as T, it can be shown from continuity and conservation of momentum that the depth change Δh at any point along the fence is given by:

$$\frac{1}{2}\left(\frac{\Delta h}{h}\right)^3 - \frac{3}{2}\left(\frac{\Delta h}{h}\right)^2 + \left[1 - Fr^2\left(1 - \frac{T}{\rho h \bar{u}^2}\right)\right]\frac{\Delta h}{h} - Fr^2\frac{T}{\rho h \bar{u}^2} = 0, \tag{2.1}$$

where $Fr = \bar{u}/\sqrt{gh}$ is the local Froude number, and h and $\bar{u}$ are, respectively, the water depth and depth-averaged velocity normal to the fence at the location of the point.

The available power generated by the device producing this force is estimated using actuator disc theory [5]. Using this approach, the force per unit length of fence, T, and the total power extracted by the turbines per unit length of fence, P_e, are written as

$$T = \frac{C_T B}{2}\rho h \bar{u}^2 \tag{2.2}$$

and

$$P_e = \rho g \bar{u}\frac{\Delta h}{h}h^2\left(1 - Fr^2\frac{1 - (1/2)(\Delta h/h)}{(1 - \Delta h/h)^2}\right), \tag{2.3}$$

where the blockage ratio, B, is defined as the proportion of the cross section of the channel swept by turbines and C_T is a local thrust coefficient for the turbine. The local thrust coefficient can be written functionally as $C_T(Fr, B, \alpha_4)$, where α_4 is the wake velocity coefficient and is defined as the ratio of the velocity in the near wake of the turbine to that immediately upstream of the turbine (figure 3).

The available power P_a is a fraction of the extracted power and is given to good approximation by:

$$P_a \approx \alpha_2\left(1 - \frac{1}{2}\frac{\Delta h}{h}\right)P_e, \tag{2.4}$$

where α_2 is the ratio of the velocity of the fluid as it passes through the turbine to the velocity upstream.

The numerical implementation and verification of this procedure into the DG ADCIRC code is described by Serhadlıoğlu *et al.* [22]. In this implementation of tidal turbines, the blockage is based on that at mean sea level, i.e. the area of the turbine remains the same, causing a small change in blockage over the tidal cycle as the water level rises and falls. The Froude number is high in shallow water areas where the flow is very fast. For high blockage ratios, this

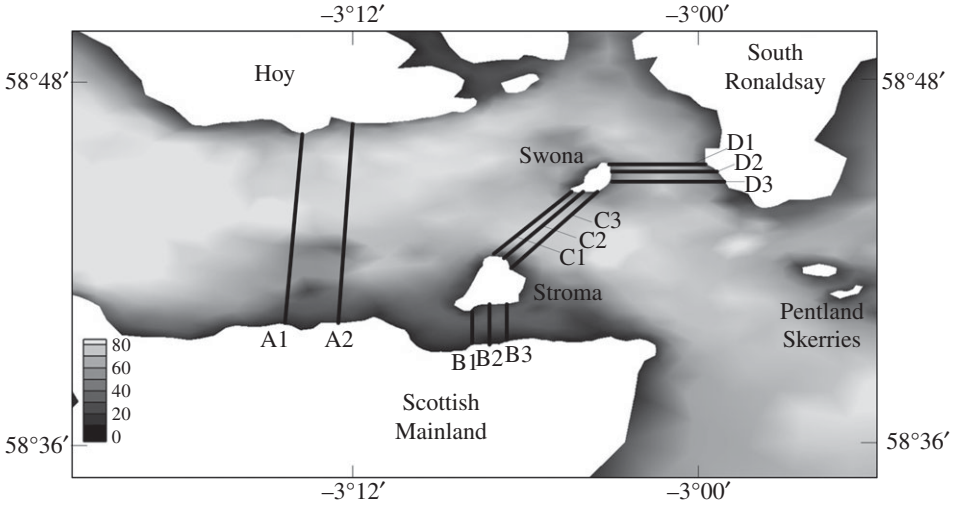

Figure 4. Location of the turbine rows considered in this study. The plot shows the water depth in metre.

can lead to the flow bypassing the turbine becoming supercritical [23,24]. To prevent this, the turbine size was reduced in shallow water areas where the depth was less than 12 m (in practice, these areas are probably too shallow to have turbines deployed), with the turbine size set to zero for depths less than 5 m. Typically, this adjustment reduced the swept area of turbines by less than 1%.

This study considers rows of turbines distributed across several locations as depicted in figure 4. The locations have been chosen as favourable for deployment of tidal stream devices noting that no thorough optimization of these locations has yet been undertaken. The first three rows of turbines are located across the narrowest section of the Pentland Firth in the three subchannels formed between the islands of Swona and Stroma (B1, B2, B3, C1, C2, C3, D1, D2, D3). Hydrodynamically, these appear optimal as the kinetic flux is largest and so fewer turbines are required to generate a given amount of power. Ample distance has been left between the rows to avoid wake–turbine interaction and to allow for maintenance. It may be possible (particularly in the shallower Inner Sound (B1, B2, B3)) to have more rows than considered here. Rows of turbines are also considered between Hoy and mainland Scotland (A1, A2).

The analysis is not dependent on a particular geometry of turbine within the rows, but rather on the cross-sectional area they occupy. Converting this cross-sectional area to a number of turbines requires an assumption about the type of turbine, because a horizontal axis water turbine will occupy a very different area per turbine than an axial flow device. However, to enable interpretation of the blockage ratios adopted herein, the blockage ratio for axial flow turbines deployed side-by-side across the channel width is taken to be

$$B = \frac{(\pi D^2/4)}{Dh} = \frac{\pi D}{4h}, \tag{2.5}$$

where D/h is the ratio of device diameter, D, to local water depth, h. Consequently, blockages of 0.1 and 0.4 correspond to devices occupying between at least 13% and 50% of the local water depth, respectively.

We do not consider non-homogeneous deployment of turbines, as discussed in Nishino & Willden [25]. This is because non-homogeneous deployments are likely to have lower basin efficiency for a given turbine area and turbine force, and so are likely to generate less available power.

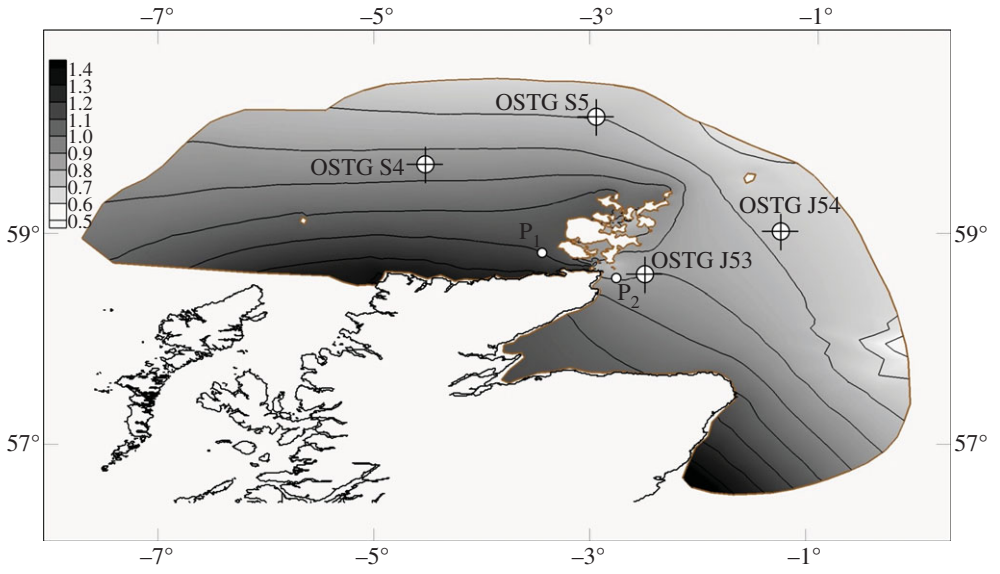

Figure 5. M_2 water level amplitude across domain (m). The measurements used in the validation are shown (white circles with cross) along with the locations used for estimating the head difference across the Pentland Firth (P1 and P2). (Online version in colour.)

3. Model validation

Before the tidal devices were inserted, the numerical model was refined and predicted water surface elevations and tidal currents compared with field observations. To facilitate this validation, in each computational run, the model was allowed to spin up from still water conditions for 1.5 days or more prior to recording any numerical results. Spinning up the model for more than a day led to negligible further changes in water surface elevation or depth-averaged velocity.

(a) Water surface elevation

Predicted water surface elevations were analysed using harmonic analysis using the inbuilt code in ADCIRC. Figure 5 shows the amplitude of the M_2 tidal constituent elevation throughout the domain. This is in excellent visual agreement with results from other models such as Sinha & Pingree [26] and Kwong & Davies [27]. Agreement for phase and for other tidal components such as S_2 (not shown) is equally good.

In assessment of tidal power, it is of prime importance that the correct water level differences across the Pentland Firth be predicted. The model predictions are therefore compared against field data at offshore locations shown in figure 5. Table 1 shows the excellent agreement between the predicted and observed M_2 elevation amplitudes given in Sinha & Pingree [26]. Furthermore, numerical tests demonstrated that the free surface elevation results are relatively insensitive to the choice of bed friction parameter.

(b) Tidal currents

To validate the numerical model for tidal currents, model results were compared with measured data of duration 30 days obtained from seabed acoustic Doppler current profiler (ADCP) gauges deployed at three locations in the Pentland Firth (see figure 6 for locations). Full details of the methodology and analysis of the field data are given in Gardline Surveys [28]. Unfortunately,

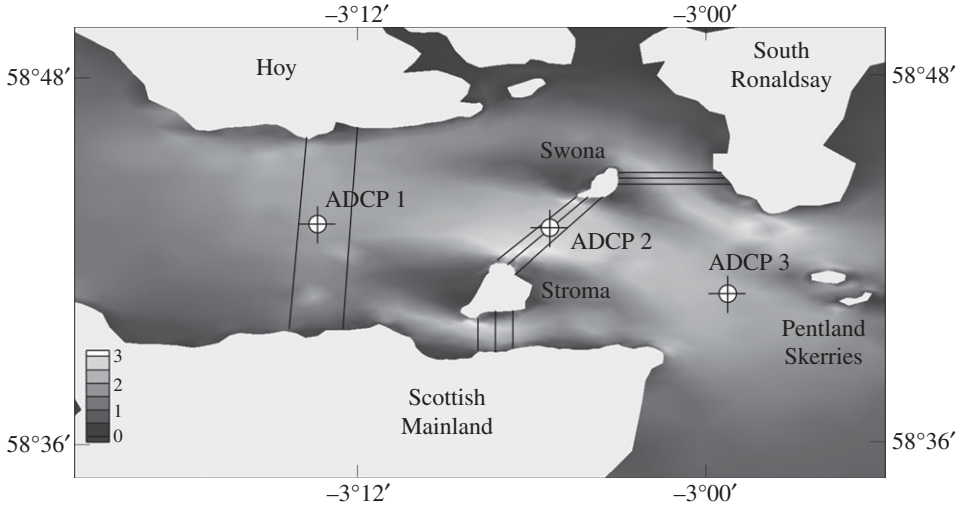

Figure 6. Contours of M_2 major axis currents predicted by the depth-averaged numerical model. The locations of the ADCP field observations of currents used in the validation are shown. The locations of the turbine rows used in this study are indicated by solid lines.

Table 1. Comparison of M_2 water level amplitudes. Amplitude in metres and phase in degrees.

	lat.	long.	observed amplitude	observed phase	model amplitude	model phase
OSTG S4	59.78	−4.65	0.83	228	0.83	229
OSTG S5	60	−2.967	0.69	252	0.70	255
OSTG J53	58.62	−2.433	0.75	323	0.79	326
OSTG J54	58.93	−1.25	0.66	323	0.68	324

only the harmonic analysis products (e.g. tidal constituent amplitude and phase) of these data were available to the authors for the present analysis. Harmonic analysis of ADCP measurements was reported at depths of 9 m, 36 or 37 m, and 65 m for each location. The three locations all had mean water depths of approximately 80 m, and so the measurement depths provide a good representation of the variation through the water column. For comparisons against the numerical model predictions in this paper, the M_2 and S_2 depth-averaged velocities were reconstructed by the authors by fitting a power law profile to the ADCP data at each location, on the assumption that the currents were in phase throughout the water column (which appears to be the case to within measurement noise, based on the phase output of the harmonic analysis). As noted by Godin [29], time series reconstructed from harmonic analysis can show poor agreement with field measurements. However, the measured data used here typically had a residual variance after removal of harmonic components whose variance was less than 10% that of the raw measurements, limiting the potential for disagreement between the predicted and measured results although we note that a 10% error in velocity would imply a greater than 10% error in kinetic energy flux.

Tables 2 and 3 list the measured data and model predictions of tidal current for M_2 and S_2 components, respectively. Both the magnitude and the phase of the tidal current are sensitive to the bed friction coefficient, in accordance with the analysis of an idealized channel by Garrett & Cummins [3].

Taken overall, the model reproduces tidal currents which have approximately the same magnitude and phase as the field measurements. No value of bed friction coefficient provides results fully in agreement with the observations. In general, the dominant streamwise current

Table 2. Characteristics of observed and predicted M_2 currents, the latter for varying bed friction coefficient.

location	observed magnitude	model magnitude			
		$C_d = 0.0025$	$C_d = 0.004$	$C_d = 0.005$	$C_d = 0.0075$
current magnitude (m s^{-1})					
1	1.70	1.67	1.60	1.54	1.36
2	2.53	2.75	2.55	2.31	2.02
3	2.35	2.17	2.09	1.97	1.74
phase (°)					
1	248	243	244	245	244
2	244	253	253	248	244
3	251	258	258	251	249
eccentricity					
1	0.076	0.160	0.035	0.018	0.045
2	0.025	0.041	0.049	0.033	0.034
3	0.052	0.020	0.051	0.051	0.062
inclination (°)					
1	89	88	85	83	83
2	112	115	114	115	115
3	134	142	143	143	142

Table 3. Characteristics of observed and predicted S_2 currents, the latter for varying bed friction coefficient.

location	observed magnitude	model magnitude			
		$C_d = 0.0025$	$C_d = 0.004$	$C_d = 0.005$	$C_d = 0.0075$
current magnitude (m s^{-1})					
1	0.59	0.54	1.60	1.54	1.36
2	0.98	0.96	2.55	2.31	2.02
3	0.67	0.72	2.09	1.97	1.74
phase (°)					
1	281	281	281	283	280
2	291	291	290	287	282
3	296	296	292	290	285
eccentricity					
1	0.074	0.020	0.050	0.023	0.029
2	0.049	0.006	0.030	0.026	0.027
3	0.070	0.000	0.059	0.042	0.005
inclination (°)					
1	86	93	89	88	84
2	125	113	113	115	115
3	132	139	142	141	142

magnitudes (roughly in the east–west direction) are better matched by a smaller value of bed friction parameter, whereas the phases typically present better agreement with higher values of bed friction parameter. In interpreting the best fit, emphasis is placed on the phase of the current as this is less likely to be sensitive to measurement noise or bathymetric errors. As a compromise, a value of bed friction coefficient of 0.005 is selected. However, because of the uncertainty in this parameter, the sensitivity of results to the bed friction coefficient is further examined in §8*a*.

We have also compared the phase of the current with the phase of several impeller current meter readings towards the west end of the Pentland Firth. These show similar agreement with the results presented in table 2. Unfortunately, the measurements were taken close to the seabed, so comparison with the magnitude of the measured current would not yield any robust information, because extrapolating this to a depth-averaged current depends on the exact profile of the boundary layer which is unknown.

Finally, the model predictions of currents are in satisfactory agreement with those shown in the Tidal Stream Atlas [30] throughout the tidal cycle, and for all the different areas of the Pentland Firth. The only exception to this is in the channel between Swona and South Ronaldsay, where the present model predicts 25% lower velocities than the Tidal Stream Atlas during the flood tide for both spring and neap cycles.

4. Extractable power

An upper bound estimate of power potential for a tidal channel has been derived theoretically by Garrett & Cummins [3] and shown to agree well with predicted values from numerical models of actual tidal channels [31,32]. Using the same depth-averaged model as used herein, the maximum extractable power in the Pentland Firth owing to forcing from the M_2 and S_2 tides has been calculated by Draper *et al.* [33] to be 4.2 GW averaged over the tidal cycle. This power estimate is slightly larger than the value predicted using the method of Garrett & Cummins [3]; the discrepancy may be attributed to a small increase that occurs in the head difference across the channel when the flow through the Pentland Firth is impeded by turbines. The increase in head is caused by a change to the phase of the tidal elevation either end of the Pentland Firth. This, in turn, drives a higher flow through some of the other channels through the Orkney Islands, but it does not cause any appreciable change to the flow to the north of the Orkneys.

In practice, it is not possible to remove all extractable power from a tidal channel without an unrealistically large number of rows of tidal turbines, as at a certain threshold the cost of adding these rows is likely to outweigh the incremental benefit in terms of any additional power generation. Section 5 considers this threshold in the context of the Pentland Firth, and presents a means of estimating the power which can be removed for generation up to the threshold.

5. Available power

(a) Time-series analysis methodology

Vennell [7] has shown that for a given blockage ratio and number of rows of turbines there is an optimal wake velocity coefficient, α_4, that maximizes the available power in a tidal channel. This optimum coefficient depends on the type of tidal channel (i.e. the geometry and natural dynamic balance) and the arrangement of the devices. It is therefore not known *a priori* what value of wake velocity coefficient α_4 will maximize the available power in the Pentland Firth although the optimum value will lie between the Lanchester–Betz limit ($\alpha_4 = \frac{1}{3}$) and unity [7]. It is also likely that the optimum α_4 will change over the spring–neap cycle because, as Draper *et al.* [33] have shown, the natural dynamic balance of the Pentland Firth varies over the same cycle. To obtain the optimum available power, model simulations were therefore undertaken for a variety of wake velocity coefficients and the time-varying available power computed in each case in order to interpolate a time-varying optimum wake velocity coefficient. More specifically, for each value of wake velocity coefficient, the time-varying available power was low-pass filtered,

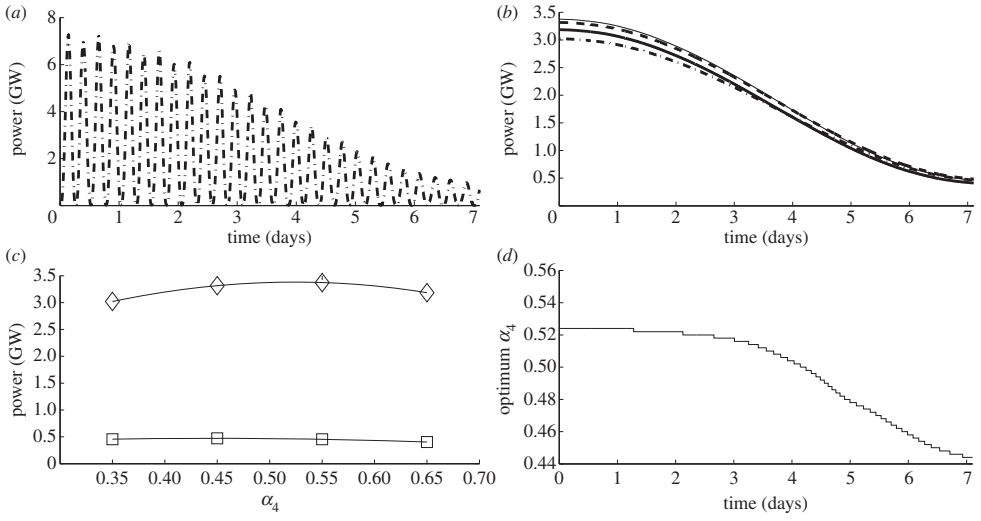

Figure 7. Example analysis over the tidal cycle. (*a*) Raw available power for $\alpha_4 = 0.35$; (*b*) low-pass filtered power for $\alpha_4 = 0.35$ (dashed-dotted line), $\alpha_4 = 0.45$ (dashed line), $\alpha_4 = 0.55$ (thin line), $\alpha_4 = 0.65$ (thick line); (*c*) available power at spring (diamonds) and neap tide (squares) and spline fit and (*d*) optimum α_4 over tidal cycle.

so as to average the result over approximately an M_2 tidal period. Every minute, the optimum filtered available power and wake velocity coefficient were then interpolated (using a spline) from the available power estimates obtained for each of the wake velocity coefficients. (This approach assumed that changes in the wake velocity coefficient over the spring–neap cycle are sufficiently small and gradual that only the magnitude of the coefficient, and not its variation, affects the tidal dynamics within the Pentland Firth at any given time.) Finally, the maximum time-averaged available power owing to M_2 and S_2 tides was calculated by taking the average over half of the spring–neap cycle.

To illustrate the methodology used to analyse the data, consider the case where there are three rows of turbines at B1, B2, B3, C1, C2, C3 and D1, D2, D3 with $B = 0.4$. Simulations have been undertaken for $\alpha_4 = 0.35, 0.45, 0.55$ and 0.65. Figure 7*a* shows the raw available power output for $\alpha_4 = 0.35$. Figure 7*b* presents the available power in the first half of the spring–neap cycle after low-pass filtering, for each value of wake velocity coefficient, as a function of time. Figure 7*c* shows splines fitted to the available power for varying α_4 at the extremes of spring tide and neap tide. The wake velocity coefficient that maximizes the available power through the spring–neap cycle is shown in figure 7*d*.

It should be noted that the same (time-varying) wake velocity coefficient is applied to all turbines in a given simulation. A slightly larger power output might be obtained by using different wake velocity coefficients in different rows (although this is likely to be small for the relatively high optimum values of α_4 calculated herein; see [8]) and, indeed, different wake velocity coefficients across rows. However, such optimization is outside the scope of this study.

(b) Turbine rows extending across whole of Pentland Firth

A deployment parameter study has been undertaken concerning the available power when up to five rows of turbines extended across the entire Pentland Firth. Deployments with a single row of turbines are located at B1, C1 and D1 (figure 4). Deployments comprising two rows of turbines are considered at B1, B2, C1, C2, D1 and D2. Deployments of three rows of turbines are investigated at B1, B2, B3, C1, C2, C3, D1, D2 and D3. When four or five rows are considered, the turbines are placed at the same locations as for the three rows, and also at A1, and A1 and A2. The blockage ratios considered represent moderate ($B = 0.1$), high ($B = 0.25$) and very high

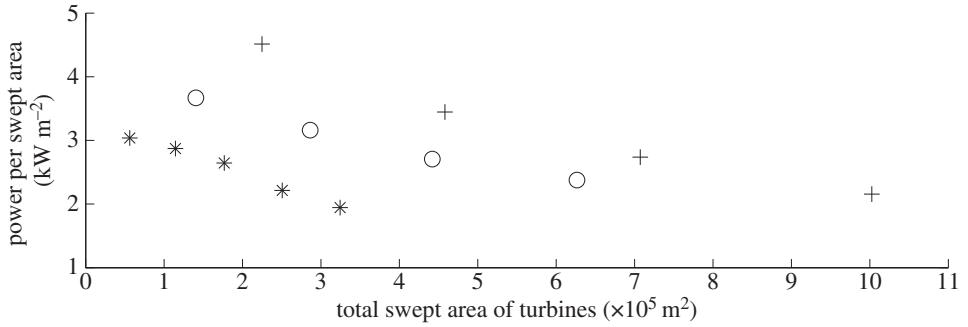

Figure 8. Time-averaged power per swept area as a function of total swept area. Plus sign, $B = 0.4$; circles, $B = 0.25$; asterisks, $B = 0.1$.

Table 4. Computed available power estimates obtained in deployment parameter study. In each case, the rows extend across the entire Pentland Firth.

no. rows	B	time-averaged available (GW)	incremental power per additional row (GW)	mean time-averaged power per swept area (kW m^{-2})	incremental power time-averaged per swept area (kW m^{-2})
1	0.4	1.01	1.01	4.5	4.5
2	0.4	1.58	0.57	3.4	2.4
3	0.4	1.94	0.36	2.7	1.4
4	0.4	2.16	0.22	2.2	0.75
1	0.25	0.52	0.52	3.7	3.7
2	0.25	0.91	0.39	3.2	2.7
3	0.25	1.20	0.29	2.7	1.9
4	0.25	1.49	0.29	2.4	1.6
1	0.1	0.17	0.17	3.0	3.0
2	0.1	0.33	0.16	2.9	2.7
3	0.1	0.47	0.14	2.6	2.2
4	0.1	0.56	0.09	2.2	1.2
5	0.1	0.63	0.08	1.9	1.1

($B = 0.4$) blockage scenarios. In all cases, the maximum time-averaged available power quoted is the average value given by the analysis technique described in §5*a*. Table 4 summarizes the resulting power estimates, from which it is obvious that the power available for generation increases as additional rows of turbines are added. There is also greater available power, for a given number of rows, when a larger blockage ratio is used. However, there is a diminishing return as additional rows are deployed—two rows of turbines produce less than twice the power of one row of the same turbines [9].

To determine the number of rows which might be viable, we now adopt the metric of time-averaged available power per swept area of turbine. An advantage of this approach is that results can be placed in context by comparison with a typical offshore wind turbine. For offshore locations around the UK, the time-averaged available power of a wind turbine varies from around 0.25 to 1 kW m^{-2} [34]. To be viable, a tidal turbine must deliver substantially greater power per swept area than a wind turbine at the upper end of this range. Figure 8 plots the time-averaged available power per swept area as a function of the total swept area of turbine deployed.

Table 5. Parameter study: mean available power for different number of rows and location of turbines in the Pentland Firth.

rows	B	mean available power (GW)
B1	0.1	0.011
C1, D1	0.1	0.159
B1, C1, D1	0.1	0.171
B1, B2, B3	0.4	0.10
C1, C2, C3, D1, D2, D3	0.4	1.76
B1, B2, B3, C1, C2, C3, D1, D2, D3	0.4	1.94

In accordance with table 4, this plot shows that (i) less power is available per swept area as additional rows of turbines are added and (ii) for a given total swept area of turbine, it is desirable hydrodynamically to use as high a blockage ratio as possible.

In terms of the power per swept area, it is useful to consider how much extra power is available when an additional row of turbines is added. For instance, if a development had three rows with $B = 0.4$ and an additional row was added this would produce only an extra 220 MW over the tidal cycle, meaning that the increase in power per additional swept area of turbines is only $0.75\,\mathrm{kW\,m^{-2}}$. This is lower than the present $1\,\mathrm{kW\,m^{-2}}$ upper limit for an offshore wind turbine, and so it is unlikely that more than 1.9 GW of power would be generated. However, the power per swept area for the first three rows producing a total of 1.9 GW is much greater than that of an offshore wind turbine.

(c) Turbines in subchannels of the Pentland Firth

It may be desirable not to place turbines across the entire channel width of the Pentland Firth in order to leave shipping lanes free, or because of a preference to develop the site in stages so that only certain locations are blocked at a particular time. Draper *et al.* [35] found that the total extractable resource was sensitive to whether the parallel subchannels formed by the islands of Swona and Stroma are, or are not, blocked by rows of turbines. These results were qualitatively consistent with the findings of Sutherland *et al.* [31] for a different tidal channel.

Because one of the first areas of the Pentland Firth which is likely to be developed is the Inner Sound (location B), we choose to investigate the likely interaction between this subchannel and those to the North of Swona. Table 5 summarizes the time-averaged available power predicted by the numerical model when turbines are deployed across B and not across C and D, or across C and D but not B. From table 5, it is clear that when a single row of low blockage turbines (i.e. $B = 0.1$) is deployed in the Pentland Firth the sum of the power available when turbines are placed solely at B, or at C and D, is nearly identical to the total power available when turbines are simultaneously deployed across all rows. This is simply because a single row at each location leads to minimal disruption to the flow. For three rows of turbines with a much higher blockage of $B = 0.4$, there is a larger reduction in the available power (approx. 4%) when turbines are not deployed across all rows simultaneously; however, this result is of relatively low magnitude. It therefore appears, for a feasible number of turbines, that interaction effects in the Inner Sound will be small. Interaction effects will be slightly more significant at other locations, such as the subchannel between Swona and Stroma, provided turbines can be installed there.

6. Simplified channel model

This section compares predictions of available power from the depth-averaged simulations against those from a simple channel model. In practice, simplified channel models are increasingly used to estimate available power in parameter studies where computational speed is particularly important. For example, Vennell [4] carried out an analysis of the Pentland Firth using such a model.

To develop the simplified model, we first follow Garrett & Cummins [3] and assume that the tidal flow through the Firth can be approximated by a one-dimensional model satisfying the dynamic equation:

$$\frac{\partial u}{\partial t} + u\frac{\partial u}{\partial x} + g\frac{\partial \eta}{\partial x} = -C_d\frac{u|u|}{2h} - F, \tag{6.1}$$

where u is the average cross-sectional velocity at an arbitrary location along the channel, η is the elevation above still water level (which is considered to be small relative to the local mean water depth h), t is time, x is distance along the channel, g is acceleration due to gravity, C_d is the bed friction coefficient and F is a force (per unit mass) parametrizing tidal devices. At any instant, there is minimal variation in flow rate along the Pentland Firth [33], and so integrating equation (6.1) along the length of the channel gives

$$g\zeta = c\frac{\mathrm{d}Q}{\mathrm{d}t} + \left(\lambda_0 + \sum_{i=1}^{N}\frac{C_T B}{2A_i^2}\right)Q|Q|, \tag{6.2}$$

where $c = \int_0^l A^{-1}\mathrm{d}x$ and $\lambda_0 = (C_d/2)\int_0^t h^{-1}A^{-2}\mathrm{d}x + A_e^{-2} - A_0^{-2}$. In equation (6.2), $Q(t) = u(x,t)A(x)$ is the flow rate, $A(x)$ is the cross-sectional area of the channel (with the subscripts 'e' and 0 representing the exit and inlet to the channel), C_T is the local thrust coefficient and B is the blockage ratio. Following Vennell [8], the force parametrizing the turbines has been replaced by the force from N rows of homogeneously distributed tidal turbines, each contributing $F = Tw_i$, with w_i the local channel width for the ith row (equal to the ratio of the local cross-sectional area to the mean local water depth A_i/h_i) and the force T defined by equation (2.2) using actuator disc theory. Lastly, ζ in equation (6.2) is the water level difference across the two ends of the channel and can generally be approximated by a series of tidal constituents [3], so that

$$\zeta = a_0\cos(\omega_0 t) + a_1\cos(\omega_1 t) + \cdots, \tag{6.3}$$

where any phase differences between the constituents are omitted, which is valid for time-averaged power generation. Using just two constituents (i.e. the M_2 and S_2) to match the numerical simulations, and introducing the non-dimensional variables $Q' = Q\omega_0 c/ga_0$, $\lambda_0' = \lambda_0 g a_0/(\omega_0 c)^2$, $t' = \omega_0 t$, equation (6.2) then becomes

$$\cos(t') + \kappa\cos\left(\frac{\omega_1}{\omega_0}t'\right) = \frac{\mathrm{d}Q'}{\mathrm{d}t'} + \left(\lambda_0' + \sigma\sum_{i=1}^{N}\frac{C_T B}{2A_i^2}\right)Q'|Q'|, \tag{6.4}$$

where $\kappa = a_1/a_0$ is the ratio of constituent amplitudes and $\sigma = ga_0/(\omega_0 c)^2$.

Application of equation (6.4) to model the Pentland Firth requires estimates of the relative amplitude of the tidal constituents, κ, the dimensionless drag ratio λ_0' and the parameter σ. The first of these parameters was calculated by Draper *et al.* [33], who evaluated the dynamic head difference across the Pentland Firth between two locations (defined as points P1 and P2 in figure 5) using the same numerical model used herein and found that the ratio of amplitudes of the S_2 and M_2 constituents was $\kappa = a_1/a_0 = 0.42/1.32 = 0.32$. To obtain the second parameter, we note that Garrett & Cummins [3] have shown that λ_0' is dependent on the phase difference between the flow rate and the elevation difference for the principal tidal constituent. The phase difference simulated by the numerical model is reported by Draper *et al.* [33] to be 49° for the Pentland Firth, so that $\lambda_0 \sim 1$ (using fig. 4 in [3]). Finally, we estimate σ by first determining the M_2 peak natural flow rate in our numerical model (which is equal to $1.169 \times 10^6\ \mathrm{m^3\,s^{-1}}$) divided by the dimensionless peak natural flow rate for $\lambda_0' = 1.0$, calculated by solving equation (6.4) with $N = 0$ and $\kappa = 0$. This ratio gives

$$\frac{Q_{\mathrm{peak}}}{Q'_{\mathrm{peak}}} = \frac{1.169\times 10^6}{0.807} = \frac{ga_0}{\omega_0 c} = \sqrt{\sigma g a_0}. \tag{6.5}$$

This gives $\sigma = 1.6 \times 10^{11}\ \mathrm{m^4}$.

Table 6. Comparison of incremental power per swept area calculated using the simplified model and the depth-averaged numerical model. Blockage ratio in each case is 0.4.

		time-averaged available power (GW)		incremental time-averaged power per swept area (kW m^{-2})	
rows	area, A_i ($\times 10^3$ m^3)	simplified model	depth-averaged model	simplified model	depth-averaged model
1	562	0.61	1.01	2.71	4.5
2	583	0.98	1.58	1.59	2.4
3	623	1.22	1.94	0.96	1.4
4	738	1.36	2.16	0.47	0.75

We solve equation (6.4) for rows of turbines at each of the locations shown in figure 4 (using the values of A_i in table 6). However, because the Froude number in the Pentland Firth is small, we simplify our model in the same way as Vennell [7], and calculate C_T from the actuator disc model of Garrett & Cummins [36]. We again optimize the wake velocity coefficient to maximize the time-averaged available power. As in the depth-averaged model analysis, the same value of wake velocity coefficient is used for all turbines in all rows.

Table 6 summarizes the results. The simplified model consistently underestimates the available power relative to the depth-averaged model. This is primarily owing to the simplification in the distribution of the current across the Pentland Firth in the simplified model. Figure 6 shows that there are significant variations in the currents across the channel in the depth-averaged model— however, these currents are simply averaged in the one-dimensional simplified model. The averaging process leads to the simplified model underestimating the naturally occurring kinetic energy flux and, in turn, the available power for modest deployments of turbines. In fact, the naturally occurring kinetic energy flux in the simplified model is just 75% of that estimated by the depth-averaged model across the first row.

Because the extractable power is not dependent on the naturally occurring kinetic energy flux (but rather on the integrated flow and head loss across the channel), there is good agreement between the channel model of Garrett & Cummins [3] and more sophisticated models of real sites [31,33]. However, when calculating the available power, the variability in current across the cross-section limits the applicability of simple channel models. Although Vennell's [4] analysis of the Pentland Firth using a simplified model gives values of power consistent with the present depth-averaged model, it should be noted that there were differences in the estimated flow rates making the agreement coincidental.

A further reason for the underestimate of the simple channel model relative to the depth-integrated model is that the former does not account for the small increase in head across the channel when turbines are inserted.

7. Other practical considerations

(a) Variation in power over the spring–neap cycle

How the power varies over the spring/neap tidal cycle has important practical consequences for turbine operation and for energy storage (particularly as all tidal developments around UK will be exposed to the same cycle). Table 7 lists the metric of the ratio of the available power averaged over a typical daily cycle at spring tide to the power generated over a similar cycle at neap tide. The ratio varies between 7.0 and 9.7. This significant variation can be explained physically by considering two limiting cases. First, by deploying a small area of turbines in the channel minimal disturbance to the flow is introduced and the power produced is approximately

Table 7. Computed available power at spring and neap tides.

no. rows	B	daily time-averaged power at spring tide (GW)	daily time-averaged power at neap tide (GW)	spring–neap power ratio
1	0.4	1.8	0.22	8.3
2	0.4	2.8	0.37	7.5
3	0.4	3.4	0.47	7.2
4	0.4	3.8	0.53	7.0
1	0.25	0.93	0.10	9.0
2	0.25	1.6	0.19	8.5
3	0.25	2.1	0.26	8.2
4	0.25	2.7	0.32	8.4
1	0.1	0.31	0.032	9.7
2	0.1	0.60	0.065	9.3
3	0.1	0.85	0.093	9.2
4	0.1	1.0	0.11	9.5
5	0.1	1.1	0.12	9.4

proportional to the kinetic energy flux. Following Garrett & Cummins [3], and letting κ be the ratio of the naturally occurring S_2 to M_2 tidal components, the kinetic energy flux ratio at spring to neap tide varies as

$$\frac{(1+\kappa)^3}{(1-\kappa)^3}. \tag{7.1}$$

The other limiting case is for the total amount of extractable power from a channel between two basins whose water level is unaffected by the dynamics in the channel. In this case, the ratio of extractable power at spring tide to that at neap tide varies as

$$\frac{(1+1.5\beta\kappa)}{(1-1.5\beta\kappa)}, \tag{7.2}$$

where β is between 1 and $\frac{9}{16}$ depending on the properties of the channel. For the Pentland Firth, $\kappa \sim 0.35$ and so based on the simplified analysis the predicted ratio of extractable power at spring tide to that at neap tide varies between approximately 9.0 (kinetic energy limit) and approximately 1.8–3.2 (total resource limit, with $\beta = \frac{9}{16}$ or 1).

The former of the two limits given above is likely to be most relevant to feasible deployments of tidal turbines, and so the power supply from tidal devices is likely to vary significantly over a tidal cycle. This variation must be appreciated by tidal device developers. In certain cases for the Pentland Firth, the ratio of available power at spring tide to that at neap tide is slightly greater than would be expected from the kinetic energy calculation. The results also show that the ratio tends to decrease as a greater swept area of turbines is deployed in the channel, and should ultimately reach the limit defined by equation (7.2). This trend, in part, occurs, because the additional turbines exert an increased retarding force on the flow during a spring tide relative to a neap tide, and this causes a greater reduction in the kinetic energy flux at spring tide than at neap tide.

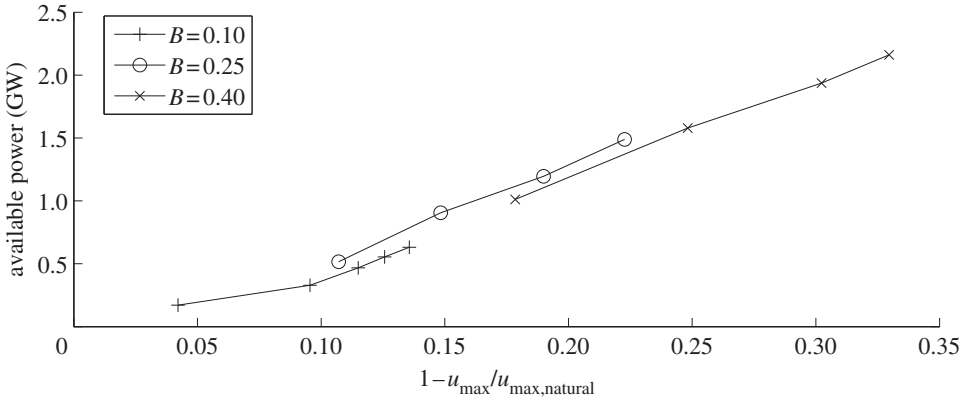

Figure 9. Change in the magnitude of the maximum current at location 58°43′01″ N, 003°05′09″ W (location 2 in figure 6) when tidal turbines are deployed to maximize time-averaged available power extraction. One to five rows (arranged as described in §2*c*) are considered for $B = 0.1$. One to four rows are considered for $B = 0.25$ and $B = 0.4$ (again in the arrangement described in §2*c*).

(b) Changes to the hydrodynamics in the Pentland Firth

The environmental consequences of placing tidal turbines in the Pentland Firth are very important in deciding whether a scheme is viable [37]. Although an in-depth analysis of the environmental changes is beyond the scope of this paper, we do comment on certain major changes to the tidal hydrodynamics.

From the analysis of the extractable power resource presented by Draper *et al.* [33], it can be seen that the major change to the hydrodynamics affects the flow passing through the Pentland Firth. Figure 9 shows the magnitude of the current at location 2 in figure 6 for different turbine configurations relative to the current in the absence of turbines. From the results, it is obvious that to remove the upper bound quoted above requires that up to a 30% change in tidal currents must be acceptable. The magnitude of the change varies between spring and neap tide and so the presence of turbines will significantly change the higher harmonics in the channel. These effects must be addressed in much more detail before any scheme can be deployed.

8. Discussion

(a) Sensitivity of results to bed friction

The bed friction coefficient is a particularly important parameter in the numerical model. In accordance with previous work on regional modelling, it had been assumed that this bed friction coefficient is constant throughout the domain. In reality, however, the coefficient is likely to vary spatially, directionally and temporally throughout the Pentland Firth, being influenced by local bed topography, bed roughness, local depth, etc. With more comprehensive field measurements of the naturally occurring currents, a more detailed picture could be built up of the variations in the bed friction coefficient—though there would inevitably remain uncertainty attached to its actual value.

To test the sensitivity of our results to the choice of bed friction coefficient, we considered two cases where the bed friction coefficient is both doubled and halved (and therefore expected to span the likely range of values at any given point). For each value of bed friction coefficient, two configurations of turbines are considered: (i) a single row of low blockage turbines and (ii) four rows of highly blocked turbines. Table 8 lists the time-averaged available power obtained for each of these cases as the bed friction coefficient is varied. As would be expected, the estimate of

Table 8. Sensitivity of available power to bed friction for two different scenarios considered in study.

		time-averaged available power (GW)		
no. rows	B	$C_d = 0.0025$	$C_d = 0.005$	$C_d = 0.01$
1	0.1	0.24	0.17	0.10
4	0.4	2.6	2.2	2.0

available power decreases as the bed friction coefficient increases. For cases with only a small area of turbines, the available power is strongly dependent on the bed friction coefficient. For large-scale deployments of turbines (close to that required for the upper-bound discussed previously), the estimate is relatively less sensitive to the value of bed friction coefficient. Even so, these results suggest that it is important that the bed friction coefficient be determined as accurately as possible, in practice, when estimating the available power from a particular deployment of turbines. Given the uncertainty (also discussed in §2) surrounding the correct value to attribute to the bed friction parameter, it should be emphasized that the estimates given in this paper should be treated with some caution, although we are confident that the results constitute best estimates.

(b) Other tidal components

This study is confined to the two principal tidal constituents. Inclusion of other tidal constituents would increase the predicted mean available power. This increase would be larger for a small number of rows of low blockage turbines than for many rows of high blockage turbines. In practice, however, it is unlikely that it will be economically feasible to extract much of this extra power, because a huge increase in the capacity of both the generators and cabling would be required to extract useful power from the additional components. Even with just M_2 and S_2 constituents, the turbines considered herein would produce an average power between approximately 0.2 and 0.25 times the peak installed capacity if 100% of the available power were to be converted into electrical power. Increasing the generating capacity so as to use the peaks in available power when other components are in phase with the M_2 and S_2 constituents would reduce the ratio of average power to peak power significantly, and place considerable demands on the performance of tidal devices.

(c) Implications for development strategy

The present strategy for developing the Pentland Firth, and other candidate tidal stream power sites, is to lease areas within the channel to different developers [38]. This strategy has been broadly successful for developing wind farms, where there is negligible interaction between different farms. However, the tidal stream resource is fundamentally different, and this paper highlights that the site must be developed as a single regulated unit, if efficient use is to be made of the tidal resource in the Pentland Firth.

Consider the scenario where a first developer has invested in a single row of turbines that are deployed across the whole Pentland Firth with a blockage of 0.4. If the developer assumes that these will be the only turbines in the Pentland Firth, the available power will be approximately 1 GW. However, if a second developer places two additional rows of turbines across the channel, then the power from the first developer's turbines will fall to approximately 0.7 GW (or less depending on how the second developer operates its turbines). Furthermore, the original row of turbines would have been designed for a higher current than will be the case once the second developer's row is deployed. This change could be very significant for devices that have been optimized for a particular range of current velocities. For example, where fatigue is critical to the

structural design, a small change in the current a turbine encounters can lead to a very significant change to the design life [39]. Thus, in this scenario, the first developer would be generating less power than anticipated, using possibly over-engineered turbines. These considerations become even more important when the turbines do not extend across the entire width of the channel, but are instead restricted solely to the subchannels within the Pentland Firth [33]. The example we have given is one in which a later development interferes destructively with an earlier development. In other scenarios, the first developer could benefit from a later development. The important point is that individual developments cannot be assessed in isolation.

9. Concluding remarks on power potential of the Pentland Firth

The maximum available power from the Pentland Firth will depend upon the maximum permissible turbine blockage and the minimum incremental power generated per swept area of turbine that is commercially viable for each new row of turbines. These limiting values are open to debate. However, taking the largest viable blockage as 0.4 and the minimum incremental power per swept area as $1\,\mathrm{kW\,m^{-2}}$ (equivalent to an offshore wind turbine), the estimated maximum available power is about 1.9 GW. To approach this level of power generation, the turbines must extend completely across the Pentland Firth, be able to accommodate large variations in power over the spring–neap cycle, and impose minimal additional drag resistance to the flow beyond that used for power generation. Moreover, changes to the flow rate through the Pentland Firth of up to 30% must also be acceptable. Further refinement of this upper bound requires many further assumptions, however, it is unlikely that a refined estimate will exceed 1.9 GW of electricity, which is already less than half of the maximum extractable power from the site calculated by Draper *et al.* [33].

Acknowledgements. S.D. kindly acknowledges support from the Lloyds Register Foundation. The Lloyd's Register Foundation supports the advancement of engineering-related education, and funds research and development that enhances safety of life at sea, on land and in the air. The suggestion to include §8c was made by one of the reviewers.

Funding statement. This work was commissioned and supported by by the Energy Technologies Institute as part of the PerAWaT project.

References

1. Carbon Trust. 2005 Phase II UK Tidal Resource Assessment. http://www.carbontrust.com/media/174041/phaseiitidalstreamresourcereport2005.pdf (accessed 5 July 2013).
2. Salter S, Taylor JRMT. 2007 Vertical-axis tidal-current generators and the Pentland Firth. *Proc. Inst. Mech. Eng. A, J. Power Energy* **221**, 181–195. (doi:10.1243/09576509JPE295)
3. Garrett C, Cummins P. 2005 The power potential of tidal currents in channels. *Proc. R. Soc. A* **461**, 2563–2572. (doi:10.1098/rspa.2005.1494)
4. Vennell R. 2013 Exceeding the Betz limit with tidal turbines. *Renew. Energy* **55**, 277–285. (doi:10.1016/j.renene.2012.12.016)
5. Houlsby GT, Draper S, Oldfield M. 2008 Application of linear momentum actuator disc theory to open channel flow. Technical report no. 2296-08, University of Oxford, Oxford, UK.
6. Draper S, Houlsby GT, Oldfield MLG, Borthwick AGL. 2010 Modelling tidal energy extraction in a depth-averaged coastal domain. *IET Renew. Power Gener.* **4**, 545–554. (doi:10.1049/iet-rpg.2009.0196)
7. Vennell R. 2010 Tuning turbines in a tidal channel. *J. Fluid Mech.* **663**, 253–267. (doi:10.1017/S0022112010003502)
8. Vennell R. 2011 Tuning tidal turbines in-concert to maximise farm efficiency. *J. Fluid Mech.* **671**, 587–604. (doi:10.1017/S0022112010006191)
9. Vennell R. 2012 Realizing the potential of tidal currents and the efficiency of turbine farms in a channel. *Renewable Energy* **47**, 95–102. (doi:10.1016/j.renene.2012.03.036)
10. Vennell R. 2012 The energetics of large tidal turbine arrays. *Renew. Energy* **46**, 210–219. (doi:10.1016/j.renene.2012.04.018)

11. Kubatko EJ, Westerink JJ, Dawson C. 2006 hp discontinuous Galerkin methods for advection dominated problems in shallow water flow. *Comp. Methods Appl. Mech. Eng.* **196**, 437–451. (doi:10.1016/j.cma.2006.05.002)
12. Kubatko EJ, Bunya S, Dawson C, Westerink JJ, Mirabito C. 2009 A performance comparison of continuous and discontinuous finite element shallow water models. *J. Sci. Comput.* **40**, 315–339. (doi:10.1007/s10915-009-9268-2)
13. Dawson C, Kubatko EJ, Westerink JJ, Trahan C, Mirabito C, Mickoski C, Panda N. 2011 Discontinuous Galerkin methods for modeling hurricane storm surge. *Adv. Water Resour.* **34**, 1165–1176. (doi:10.1016/j.advwatres.2010.11.004)
14. Parker BP (ed.) 1991 *Tidal hydrodynamics*. London, UK: John Wiley.
15. Stansby PK. 2006 Limitations of depth-averaged modeling for shallow wakes. *J. Hydraul. Eng.* **132**, 737–740. (doi:10.1061/(ASCE)0733-9429(2006)132:7(737))
16. Adcock TAA, Borthwick AGL, Houlsby GT. 2011 On the open boundary problem in basin modelling of tidal energy extraction with application to the Pentland Firth and the Bristol Channel. In *EWTEC 2011, Southampton, UK, 5–9 September 2011*.
17. le Provost C, Lyard F, Molines JM, Genco ML, Rabilloud F. 1998 A hydrodynamic ocean tide model improved by assimilating a satellite altimeter-derived data set. *J. Geophys. Res.* **103**, 5513–5529. (doi:10.1029/97JC01733)
18. Garrett, C. & Greenberg, D. 1977 Predicting changes in tidal regime: the open boundary problem. *J. Phys. Oceanogr.* **7**, 171–181. (doi:10.1175/1520-0485(1977)007<0171:PCITRT>2.0.CO;2)
19. Rainey RCT. 2009 The optimum position for a tidal power barrage in the Severn estuary. *J. Fluid Mech.* **636**, 497–507. (doi:10.1017/S0022112009991443)
20. Baston S, Harris RE. 2011 Modelling the hydrodynamic characteristics of tidal flow in the Pentland Firth. In *EWTEC 2011, Southampton, UK, 5–9 September 2011*.
21. Easton MC, Woolf DK, Bowyer PA. 2012 The dynamics of an energetic tidal channel, the Pentland Firth, Scotland. *Cont. Shelf Res.* **48**, 50–60. (doi:10.1016/j.csr.2012.08.009)
22. Serhadlıoğlu S, Houlsby GT, Adcock TAA, Draper S, Borthwick AGL. 2013 Assessment of tidal stream energy resources in the UK using a discontinuous Galerkin finite element scheme. In *17th Int. Conf. on Finite Elements in Flow Problems, San Diego, CA, 24–27 February 2013*.
23. Whelan JI, Graham JMR, Peirò J. 2009 A free-surface and blockage correction for tidal turbines. *J. Fluid Mech.* **624**, 281–291. (doi:10.1017/S0022112009005916)
24. Draper S. 2011 Tidal stream energy extraction in coastal basins. DPhil thesis, University of Oxford, Oxford.
25. Nishino T, Willden R. 2012 The efficiency of an array of tidal turbines partially blocking a wide channel. *J. Fluid Mech.* **708**, 596–606. (doi:10.1017/jfm.2012.349)
26. Sinha B, Pingree RG. 1997 The principal lunar semidiurnal tide and its harmonics: baseline solutions for M2 and M4 constituents on the northwest European continental shelf. *Cont. Shelf Res.* **17**, 1321–1365. (doi:10.1016/S0278-4343(97)00007-1)
27. Kwong SCM, Davies AM. 2001 A three dimensional model of the M2, S2, N2, K1 and O1 tides in the Faeroe–Shetland channel. *Cont. Shelf Res.* **21**, 1263–1297. (doi:10.1016/S0278-4343(01)00005-X)
28. Gardline Surveys 2001 Pentland Firth tidal stream observations. Technical Report no. 5699. Gardline Surveys.
29. Godin G. 1983 On the predictability of currents. *Int. Hydrogr. Rev.* **60**, 119–126.
30. Admiralty 1986 *Tidal stream atlas Orkney and Shetlands*, 4th edn. NP209. Taunton, UK: Hydrographic Office.
31. Sutherland G, Foreman M, Garrett C. 2007 Tidal current energy assessment for Johnstone strait, Vancouver Island. *Proc. Inst. Mech. Eng. A, J. Power Energy* **221**, 147–157. (doi:10.1243/09576509JPE338)
32. Karsten RH, McMillan JM, Lickley MJ, Haynes RD. 2008 Assessment of tidal current energy in the Minas passage, Bay of Fundy. *Proc. Inst. Mech. Eng. A, J. Power Energy* **222**, 493–507. (doi:10.1243/09576509JPE555)
33. Draper S, Adcock TAA, Borthwick AGL, Houlsby GT. Submitted. The extractable power from the Pentland Firth. *Renew. Energy*.
34. DTI 2004 Atlas of UK marine renewable energy resources. 2008. ABPmer. Technical report no. R.1106, Department of Trade and Industry. http://www.renewables-atlas.info (accessed 27 June 2013).

35. Draper S, Adcock TAA, Borthwick AGL, Houlsby GT. Submitted. An electrical interpretation of the Pentland Firth tidal stream power resource. *Proc. R. Soc. A*.
36. Garrett C, Cummins P. 2007 The efficiency of a turbine in a tidal channel. *J. Fluid Mech.* **588**, 243–251. (doi:10.1017/S0022112007007781)
37. Shields M, Dillion I, Woolf D, Ford A. 2009 Strategic priorities for assessing the ecological impacts of marine renewable energy devices in the Pentland Firth (Scotland, UK). *Marine Policy* **33**, 635–642. (doi:10.1016/j.marpol.2008.12.013)
38. Crown Estates 2011 Wave and tidal energy in the Pentland Firth and Orkney waters: how the project could be built? Report by BVG Associates.
39. McAdam R. 2011 Studies into the technical feasibility of the transverse horizontal axis water turbine. DPhil thesis, University of Oxford, Oxford.